 doi:10.20944/preprints202208.0512.v1

Article

Snow Contact Characterisation of Cross-country Skis: a Macro-scale Study of the Apparent Contact

Kalle Kalliorinne*[1], Joakim Sandberg[1], Gustav Hindér[1], Roland Larsson[1], Hans-Christer Holmberg[2] and Andreas Almqvist[1]

[1]*Division of Machine Elements,*
[2]*Division of Health, Medicine and Rehabilitation,*
Luleå University of Technology, SE97187, Luleå, Sweden

**Corresponding author*

Abstract: In cross-country skiing the time difference between a race winner and the person coming second is typically very small. Since much of the energy is spent on overcoming resistive forces, a relatively small reduction of these can have a significant impact on the results. The resistive forces come partly from the friction in the tribological interface, between the ski and the snow, and as with many tribological applications the characterisation of its origin, plays an important role in determining the frictional properties. Also in cross-country ski friction, there are several scales impacting the frictional performance, with the major contributors being the ski-camber profile and ski-base structure. Macro-scale measurements of the ski's camber profile under load, are often used to determine how adequate the ski is for a specific condition. The characteristic properties usually obtained are, the force required to collapse the ski to a certain camber height, the topography of the kick-wax zone, and by simple means a determined lengths of the frictional interface, i.e., the apparent contact length. To this date, there are some mathematical models, but there is no robust way of determining the macro-scale contact properties between a cross-country ski and a counter surface using simulations. In the present paper an Artificial neural network (ANN) is trained to predict the ski-camber profile for various loads placed at different positions, and a well established deterministic approach is used to simulate the contact between the ANN-predicted ski-camber profile and a linearly elastic body with a flat surface, representing the snow. The results suggest that this method is feasible for the determination of the apparent contact characteristics of different skis. Moreover, we show that the apparent contact area does not linearly depend on the load, and that the elastic properties of the counter surface also has a large impact on the apparent contact area and the average apparent contact pressure.

Keywords: Contact Mechanics; Cross-Country Skiing; Cross-Country Ski; Load Conditions; Ski-Camber Profile; Sports Equipment

 doi:10.20944/preprints202208.0512.v1

Nomenclature

E_{base}	Elastic modulus of the ski base	Pa
$E_{counter}$	Elastic modulus of the counter material	Pa
E'	Equivalent elastic modulus	Pa
ν	Poisson ratio	Pa
h	Ski-camber height	m
m	Load magnitude	kg
x_m	Loading position	m
x	x-coordinate	m
p	Apparent contact pressure	Pa

1 Introduction

In the winter Olympics, solid-phase water is present in some way in every sport. Some sports are practised on top of ice, and in these the contacting surface of the sports equipment is made of steel. Other are practised on snow, where the sports equipment's contacting surface is often made of a polyethylene, and in alpine skiing good control is achieved by the addition of steel edges to the polyethylene ski base with low gliding friction. Friction on snow has fascinated researchers for years, and already in 1939, Bowden published his groundbreaking paper [1] on this topic, and since then, many publications have followed. There has have always been an interest to reduce the friction further. Eriksson [2] did for instance, study snow friction as a means to increase the transportation efficiency of timber. In 1955, Bowden [3] started exploring friction on snow and ice, and, especially, on how to reduce ski friction. This opened the door to a fascinating research area, in which there are many active researchers today.

During the years, there have been quite many theoretical studies [4–10] that present various equations to model the friction between the ski and the snow. In order to explain what governs the friction on snow and ice, a substantial amount of research has also been committed to explore and understand the mechanisms involved, see e.g., Lever et al. [11], Scherge et al. [12] and Almqvist et al. [13] for some recent work in this direction. The different friction mechanisms, i.e., snow compaction, micro-ploughing, adhesion, viscous shearing and water bridging, see [13], have been modelled by assorted equations based on different assumptions. In most of the models available, the apparent contact pressure is assumed to be uniformly distributed over the apparent contact area. One of the most common assumptions, is that the dry real area of contact equals the load divided by the hardness of the softer of the two contacting bodies, see e.g., Glenne [4]. By definition, this gives a minimum estimate of the real contact area and of the corresponding friction force. Another assumption is that the contact area comprises all of the regions that are in close proximity of being in contact. This is the area considered when modelling the component of wet friction in many models, see e.g., Lehtovaara [5], even though it is well-known that it is countably larger than the real area of contact.

The present study serves to shed some light upon the assumptions connected to the *apparent* contact area and the corresponding *apparent* contact pressure. The apparent contact area can be considered being the contact area seen at the macro scale, and if we were looking at it at a higher magnification, e.g., from a *micro-scale* perspective, we would find that it was the ski-base structure and the grainy snow topography of the ski track that constitutes the real area of contact. This multi-scale nature, so characteristic to contact mechanics in general, has been extensively studied previously, see e.g., [14–19]. Bäurle et al. [20] studied the ski-snow interaction at the micro scale and found that the real area of contact can be as small as 10% of the apparent contact area at cold conditions, and as large as 100% at warmer conditions. Another example is provided by Mössner et al. [21], who found that the real area of contact between a single snow grain (modelled as a sphere) and the ski base was less than 3% of the apparent contact area. Finally, Scherge et al. [12], conducted numerical calculations to simulate the micro-scale contact mechanics between ice and measured ski-base topographies. The results they presented shows that the real area of contact may be

 doi:10.20944/preprints202208.0512.v1

as small as 0.1%, and that a perfectly plastic- and the more realistic elasto-plastic approximation of the material behaviour, is significant, but also that the former preserves the ranking and, therefore, may be used for a qualitative analysis. All-in-all, this indicates that the *real* contact area, typically covers only a small part of the area seen at the macro scale, suggesting that the corresponding real contact pressure may be significantly higher than the pressure estimate given by the total load divided by the apparent contact area. The contact pressure under loaded ski has been experimentally obtained by Bäckström et al. [22], Schindelwig et al. [23], and also by Kristiansen [24]. The contact pressure and area are, however, dependent on the stiffness of the counter surface and, to the authors best knowledge, there are no published results related to skiing on this relationship.

Measurements of the ski-camber profile can be used to evaluate ski properties with respect to several aspects, e.g., the force required to collapse the ski to a certain camber height, the topography of the kick-wax zone, and the lengths of the frictional interfaces, i.e., the apparent contact area. Breitschädel [25, 26] did, for example, look at the ski stiffness and its variation with temperature, and he also defined a contact criterion, based on the assumption that contact occurs wherever the ski-camber height is less than 50 µm, that he used to appreciate the length of the frictional interfaces of cross-country skis. This contact criterion was recently used by Kalliorinne et al. [27] as a measure for comparison, when they conducted contact mechanics simulations to analyse how the length of the friction interfaces varies, as the athlete executes the downhill-tucking position in different ways.

The objective of this paper is to present a method for determining the macro scale contact mechanical properties of cross-country skis, by employing a ski-camber profile measurement devise, a neural network architecture and a computational contact-mechanics model. The resulting macro scale contact mechanical properties obtained this way will, therefore, be represented by the apparent- contact pressure and area for a given loading condition as the virtual ski is put into contact with virtual snow, modelled as a linear elastic half space exhibiting arbitrary stiffness. This comprises, according to authors best knowledge, a novel method that may be used to further the state-of-the-art and to obtain useful insights about the macro-scale contact mechanics of cross-country skis, and other systems exhibiting similar behaviour.

 doi:10.20944/preprints202208.0512.v1

2 Theory

A model that governs the contact mechanical response that results when a cross-country ski is pressed against an other body, must considers the multi-scale and multi-physics nature of the processes involved. In this work the response, in terms of ski collapse/deformation and the corresponding contact pressure will be considered at three distinctly separate scales, i.e., the *macro*-, *meso*- and the *micro* scale.

Figure 1 gives a schematic view of the scales present in the contact mechanics problem resulting when a cross-country ski is pressed against another body. The scale at the bottom is the one seen by the naked eye, and it is hereafter refereed to as the macro scale. It encompasses both the ski-camber profile (blue solid line) that is in contact with the snow surface (black solid line), and the equivalent load from the athlete's bio-mechanical input to the (grey coloured) ski, through the (red coloured) ski boot, illustrated by the red arrow. The equivalent load (caused by the athlete's bio-mechanical input) has two attributes, i.e., a magnitude and a location of application, which may be used to simulate specific positions withing different cycles, e.g., during the diagonal stride or while double poling on a classic ski, or during anyone of the 7 gears used in skating [28, 29], and it is of outermost importance to consider the effect of these two parameters on the ski-camber profile.

The apparent contact pressure, illustrated with the red solid line in Fig. 1, is a feature of the meso scale, which encompasses the *contacts* at the rear- and the front-glide zones and the surface of the snow. These meso-scale sized contacts constitutes the frictional interfaces between the ski-base, illustrated by the ski-camber profile (solid blue line), and the surface of the snow (solid black line). Nota bene, i) these two profiles are presented at a 100× magnification in the vertical direction at this scale, ii) the pressure distribution is highly sensitive to irregularities and therefore highlights the out-of-flatness of the contacting surfaces at the meso scale.

Features of the micro scale are the micro topography of the ski-base structure, the corresponding real contact- pressure[1] and area are features appearing at the micro scale. In Fig. 1 the lower of the two illustrations, appearing above the magnified presentation of the ski-camber profile and the snow surface and the apparent (meso-scale) pressure distribution, depicts the ski-base topography, and the upper one the corresponding real (micro-scale) pressure distribution. Because of the magnitude of the corresponding meso-scale pressure (red solid line) the load carried by a unit area of the ski-base structure is larger at the rear glide zone than it is at the front.

[1] The surface roughness is a multi-scale process in itself, meaning that the level of magnification required to discern all important features depends on the procedure behind the making and tribological system it is operating within.

Preprints (www.preprints.org) | NOT PEER-REVIEWED | Posted: 31 August 2022 doi:10.20944/preprints202208.0512.v1

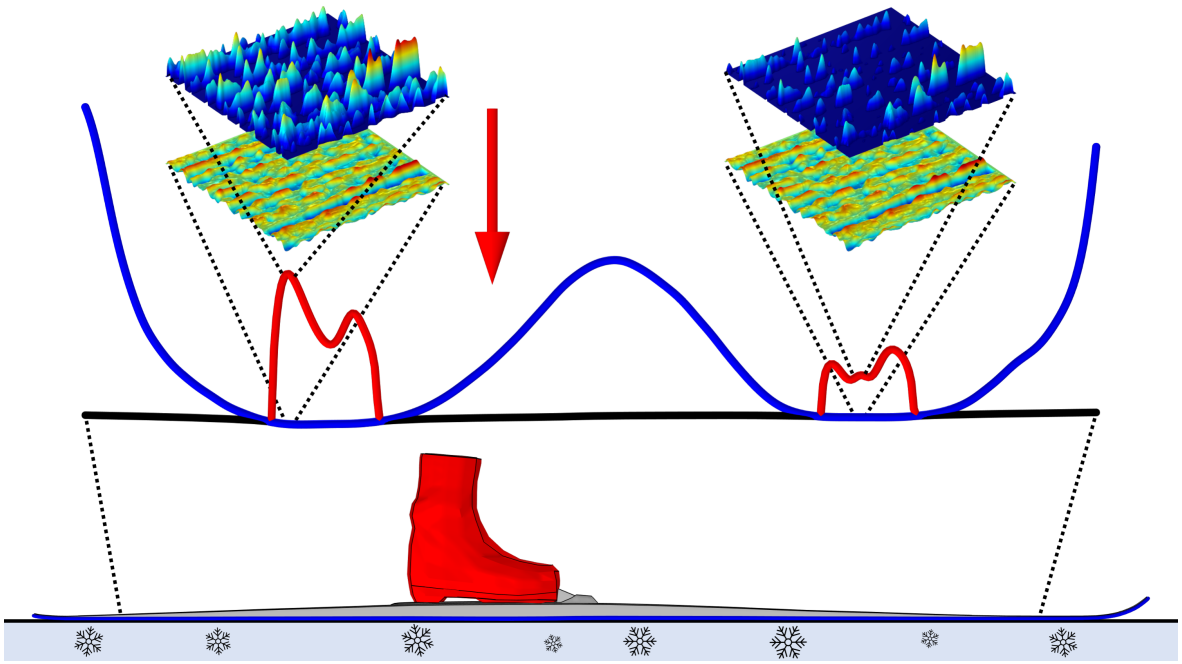

Figure 1: A schematic view of the macro-, meso- and the micro scale incorporated in the model of the contact between a cross-country ski pressed against another body. At the bottom the macro scale is illustrated, where the ski boot (coloured in red) is manifesting the athlete's bio-mechanical input to the (grey coloured) ski with a ski-base surface profile, i.e., the *ski-camber profile*, (solid blue line), which makes contact with the surface of the snow (solid black line). Another feature appearing at the macro scale, is the equivalent load from the athlete is transferred through the ski boot, which is illustrated with the red arrow. Above the macro scale, we find the meso scale encompassing the contact between the ski-base, illustrated by the ski-camber profile (solid blue line), and the snow surface (solid black line), both of which are presented at a 100× magnification in the vertical direction. At the meso scale, we also find the apparent contact pressure (solid red line), corresponding to the equivalent load from the ski boot (illustrated by the red arrow). Above the meso scale, which encompasses both the rear- and the front-glide zones, which constitute the frictional interfaces in this problem, we have two different illustration of features belonging to the micro-scale. The lower one of these illustrating the topography of the ski-base structure, and the upper the corresponding real micro-scale contact pressure.

When it come to practical application, the ski-camber profile is frequently used to determine the how suitable a particular cross-country ski is for an individual athlete at certain conditions. The ski-camber profile reveals e.g., what the camber height is, and approximately where the glide zones will appear. For a classic ski, this information is used to determine e.g., how much load that is required to collapse the ski to produce grip during the diagonal stride or while performing kick double pole technique, where kick-wax should be applied. In addition, by using Breitschädel's contact criterion, that is based on the assumption that contact occurs wherever the ski-camber height is less than 50 µm, the length of the apparent contact area of the glide zones can be estimated [26]. However, this contact criterion is based on a constant value of 50 µm of the penetration depth, i.e., how deep the ski-base sinks into the snow, implying that it would always be the same, irrespectively of the prevalent conditions. The penetration depth is, however, not a constant. It is, for sure, dependent on the properties of the ski-base material and structure, the loading

 doi:10.20944/preprints202208.0512.v1

condition, and properties of the snow. Both softer snow and ski-camber profiles exhibiting smaller apparent contact area will, for instance, result in a larger penetration depth. The ski-camber profile measurements are usually done on a plane and hard counter surface, such as the stone in the SkiSelector machine [30]. In the present analysis, it is assumed that the ski-camber profile, used as input for the contact mechanics simulations, is independent of the properties of the counter material, i.e., that the ski-camber profile would be the same if the counter surface would be made of rigid stone or soft snow.

Preprints (www.preprints.org) | NOT PEER-REVIEWED | Posted: 31 August 2022 doi:10.20944/preprints202208.0512.v1

3 Method

In the present paper, a classic- and a (free style) skate cross-country ski are used for the evaluation of the skis contact mechanical response. The first step addresses the macro-scale deformation of the ski. This involves ski-camber profile measurements, training of an Artificial neural network (ANN) and employing it to predict the deformation of the ski for a given loading condition. In the second step, the predicted ski deformation is used as input for numerical calculations, predicting the ski's contact mechanical response, in terms of the apparent *meso-scale* contact pressure and area.

3.1 Macro-scale measurement and prediction

Together with representative material data, only a single macro-scale measurement of the ski-camber profile is required as input to execute a numerical calculation of the apparent contact pressure and area that would develop at the meso-scale between the ski and the counter material. The results obtained would, however, then only represent a single loading condition, in terms of the load magnitude, m, and position, x_m. This means that a new measurement would be needed for another (if only slightly different) loading position, and this would make the procedure of tracking and predicting the contact mechanics of, e.g. a whole cycle of the diagonal stride or while double poling on a classic ski, or of anyone of the first 6 (of the 7) gears in skating, extremely inefficient. To circumvent this problem, the methodology proposed herein uses an ANN that is trained on a ski-camber profile dataset, obtained for various loads placed at different positions using a SkiSelector [30] ski-camber profile measuring device, show in Fig. 2(left). Artificial neural networks are frequently used and when successfully trained (neither under- nor over learned), an ANN, with a fit-for-purpose architecture, can be used to obtain highly accurately predictions within in the domain spanned by the training data. The training data used in the present study was collected by measuring the ski-camber profile at loads ranging from 5 kg to 130 kg, positioned between 40 mm and 240 mm behind the balance point (as indicated by the ski manufacturer), see Fig. 2(middle) for the complete specification. In this way, the ANN, with the architecture depicted in Fig. 3 and the ANNs available in MATLAB Central File Exchange [31, 32], these are capable of making predictions with a mean error smaller than 20 µm. Figure 2(right) shows the tip of the classic- and the skate ski used in this study.

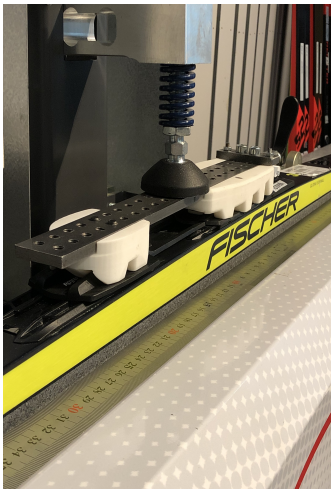

Load magnitude (m) [kg]
5 - 15 (inc. of 2.5)
20 - 65 (inc. of 5)
70 - 130 (inc. of 10)

Loading position (x_m) [mm]
−240 - −40 (inc. of 20)

Figure 2: Measurement setup using the SkiSelector [30] to retrieve the ski-camber profile, a Fischer skate ski [33] is used, equipped with the Measurement boot developed in [27] (left). Sequences for loading, in terms of mass and positioning relative to the balance point, located at $x = 0$ (middle). The tip of the classic- and skate ski used in the present work (right).

Preprints (www.preprints.org) | NOT PEER-REVIEWED | Posted: 31 August 2022 doi:10.20944/preprints202208.0512.v1

All of the measurements are combined into a large dataset consisting of 3 inputs and 1 output. The three inputs are the coordinate running along the ski x, with $x = 0$ at the balance point, paired with a loading condition represented by the mass m and the position x_m, where it is applied, and the output is the ski-camber height h. The ski-camber height h may, therefore, be defined as

$$h = f(x, m, x_m), \tag{1}$$

where f is an *a priori* unknown function. One way of realising such an unknown function, is to represent it by a carefully designed ANN. In the present work, an ANN is constructed using the deep learning toolbox in MATLAB® [34]. The final version of the ANN architecture developed herein is shown in Fig. 3. In the deep learning toolbox implementation of this ANN it is made up of 7 fully-connected hidden layers sectioned into 4 blocks.

This sectioning, with each block detailed in the list below, is adopted because of the need for passing the inputs to different stages within the network and not only to the first hidden layer.

1. The first block consist of a "Load-condition" layer that preprocesses the load condition inputs m and x_m, and the output is then passed to the second block.
2. The second block designed to handle the ski collapse, thus requiring as input both the x-coordinate and the output from the "Load-condition" block. The block consists of 3 "Ski-collapse" layers which all employ the *tansig* transfer function.
3. The third block, that governs the ski-camber processing, consists for two layers employing the *tansig* transfer function. This block only takes the x-coordinate as input, hence, making it independent of the loading condition.
4. The fourth block is the "Prediction" block, it combines the output from the "Ski-collapse" block and the "Ski-camber" block, to make the prediction. This block consist of a single layer which employs the *pure-lin* transfer function. The output from this block is the received y-coordinate of the ski-camber profile under the specified load-condition.

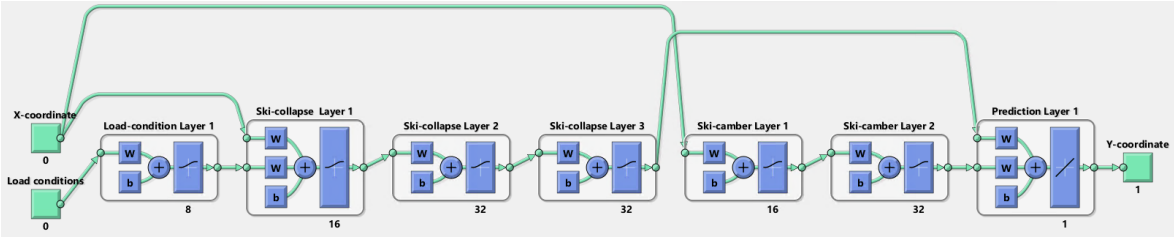

Figure 3: Architecture of the Matlab based neural network, with 3 inputs x, m and x_m, 7 hidden layers and 1 output "Y-coordinate", i.e. $h = f(x, m, x_m)$. The inputs are separated into "X-coordinate" i.e. x and "Load conditions" i.e. m and x_m. The fully-connected hidden layers are sectioned in to 4 blocks consisting of one load-condition layer, three ski-collapse layers, two ski-camber layers and one prediction layer. The input-layer, layer-layer and layer-output connections are illustrated with green arrows. All layers have *tansig* activation functions, except for the prediction layer, which has a *pure-lin* activation function.

There are several benefits from employing an ANN to model this type of system. For example, because of the relatively small amount of neurons compared to the number of parameters in the training data, the ANN will act as a filter for the small amount of noise in the measurement data. The the most significant advantage, however, is the ability of the ANN to perform highly accurate interpolation within

Preprints (www.preprints.org) | NOT PEER-REVIEWED | Posted: 31 August 2022 doi:10.20944/preprints202208.0512.v1

the parameter space spanned by the training data. In this present study, it is particularly useful for predicting the entire ski-camber profile, given an arbitrary load condition (within the specification given in Fig. 2). In addition, the ski-camber profile prediction is performed on a discrete set of x-coordinate values, which can be specified at the preferred resolution, meaning that the subsequent meso-scale calculations can be realised at required mesh resolution, independently of the original number of sampling points, collected during the ski-camber profile measurement.

3.2 Meso-scale calculation

The meso-scale contact mechanics calculations performed in this work was conducted with a deterministic Boundary element method (BEM) based contact mechanics model for the contact between two semi-infinite half spaces, developed by Almqvist et al. [35] and then further improved by Sahlin et al. [36]. Since then, the model has been employed on several occasions e.g. [37–41]. This type of dimension-reduced half-space approach, lets us consider the contact between two linearly elastically deformable bodies as the contact between one *equivalent* elastic body and a rigid plane. The elastic modulus E' of the equivalent elastic body given by

$$\frac{2}{E'} = \frac{1-\nu^2}{E_{base}} + \frac{1-\nu^2}{E_{counter}}, \tag{2}$$

where $\nu = 0.3$ is the Poisson number, E_{base} is the elastic modulus of the ski base and $E_{counter}$ is the elastic modulus of the counter surface. Lintzén and Edeskär [42] investigated uni-axial compression of snow of different types, and they estimated the Young's modulus of the snow to be between 100 and 250 MPa for new machine-made snow, and between 50 and 350 MPa for old machine-made snow. The contact mechanics calculations simulating the ski-snow contact performed in this work, are therefore conducted for Young's moduli within the range (20 MPa, 400 MPa.

In the present work, the ski-camber profile is modelled as a rigid body, i.e. calculations are made under the assumption that only the values of the load magnitude m and position x_m have an influence on the deformation of the ski-camber profile. It is also assumed that, the material of the counter body is linearly elastic, that there is no friction between the contacting surfaces, and that the height variations of the surfaces are small compared to their lateral dimensions.

An addition to the numerical solution procedure, of the BEM based model [36], was made to allow the ski to rotate around the loading point in order fulfilling both force- and moment balance, in terms of the apparent contact pressure $p(x)$ and the loading position x_m, i.e.

$$\int p(x)\,dx = mg, \quad \int (x + x_m)p(x)\,dx = 0. \tag{3}$$

An initial test of the modified contact mechanics model, was carried out to ascertain its feasibility. To this end, a model problem resembling the SkiSelector [30] was configured. Both a classic and a skating ski with measured ski-camber profiles was used to model the rigid bodies, which were pressed against against an elastic body with the equivalent elastic modulus $E' \approx 1.96$ GPa calculated using $E_{base} = 900$ MPa and $E_{counter} = 70$ GPa, with $\nu = 0.3$. The outcome of this initial test presented in Fig. 4, which depicts both the ANN-predicted (solid blue line) and the measured (dashed black line) ski-camber profiles for both the classic and the skating ski. Since the stone counter surface is very stiff, the load will be distributed over a relatively short length of the ski. This is also reflected by the apparent contact pressure (solid red line), exhibiting spike like peaks at the narrow regions of contact.

Preprints (www.preprints.org) | NOT PEER-REVIEWED | Posted: 31 August 2022 doi:10.20944/preprints202208.0512.v1

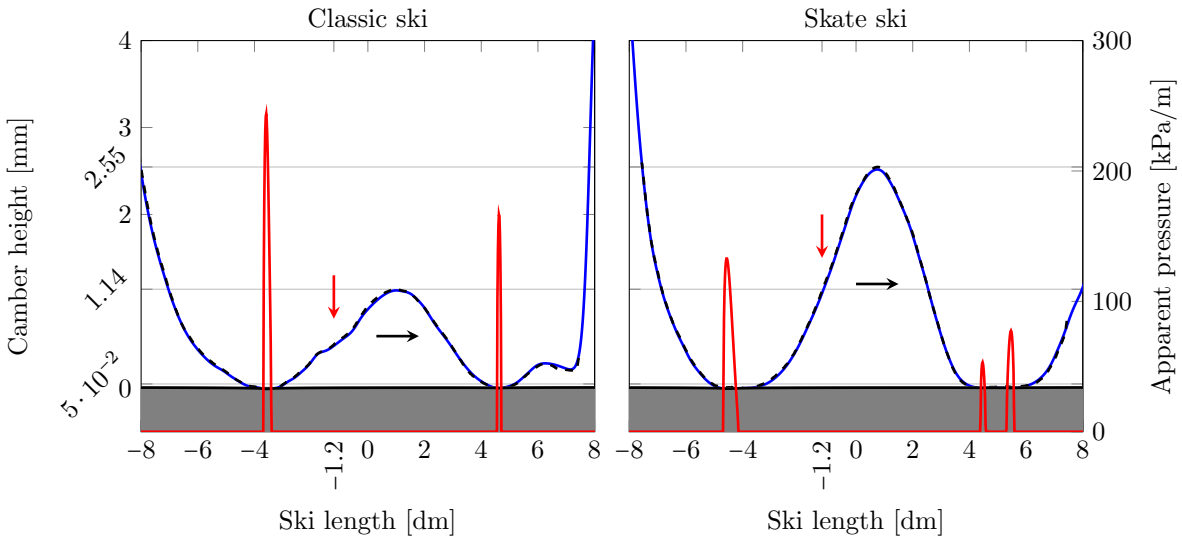

Figure 4: The ANN-predicted (solid blue line) and measured (dashed black line) ski-camber profiles of for a classic- (left) and a skate ski (right) loaded with m = 30 kg at x_m = −1.2 dm, and the corresponding apparent pressure distribution (solid red line). The vertical red arrow indicates the equivalent loading position and the horizontal black arrow the gliding direction. The elastic moduli used in the simulations are 900 MPa, for the ski base, and 70 GPa, for the stone counter surface. According to the contact mechanics calculations, the classic ski (left) have rear/front apparent contact lengths of 28.1 mm/14.9 mm with corresponding average apparent pressures of 169 kPa/137 kPa, and the skate ski (left) was predicted to have rear/front apparent contact lengths of 52.7 mm/45.7 mm with corresponding average apparent pressures of 83.7 kPa/48.1 kPa.

Preprints (www.preprints.org) | NOT PEER-REVIEWED | Posted: 31 August 2022 doi:10.20944/preprints202208.0512.v1

4 Results and Discussion

In this section results and discussion pertaining to the influence of load magnitude, position, and the stiffness of the counter surface, on the contact mechanical response will be shown. In Figures 5-7 the loaded mass m, load position x_m and elastic module of the snow counter surface $E_{counter}$ have been varied one-by-one, keeping the other two parameters constant.

Figure 5 depicts the skate ski, under two load cases represented by $m = 30\,\text{kg}$ (left) and $m = 60\,\text{kg}$ (right), for the same load position $x_m = -120\,\text{mm}$ and elastic modulus $E_{counter} = 100\,\text{MPa}$. When the load changes from 30 kg to 60 kg, the apparent contact length at the rear contact region nearly doubles, by increasing from 146 mm to 288 mm. The corresponding mean pressure does, however, only exhibit an 8.5% increase, going from 30.6 kPa to 33.2 kPa. The front contact region exhibits a completely different response. When the load is increased, the apparent contact length decreases moderately (≈18%), from one patch of 162 mm to two patches that mounts up to 132 mm, while the mean apparent contact pressure increases from 13.8 kPa to 28.9 kPa. We note that even though the overall contact topology of the ski's *frictional interface* is very different under the two load cases, the load partitioning between the rear- and front frictional interfaces remains nearly unchanged as it is 67%/33% and 71%/29%, for the 30 kg and 60 kg loads, respectively.

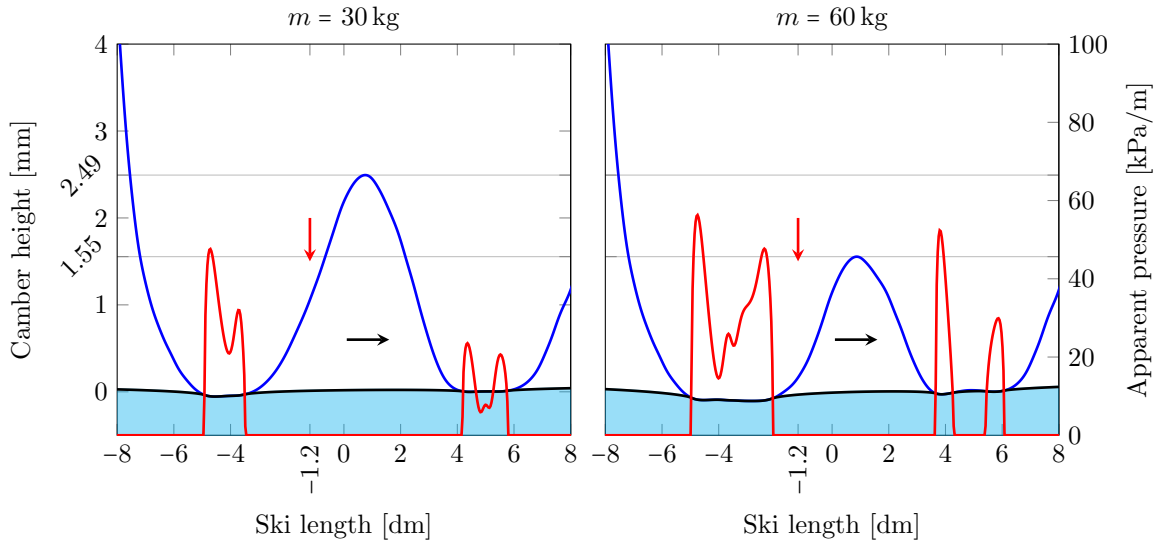

Figure 5: The skate ski under two different loads, 30 kg (left) and 60 kg (right), and the load positioned 120 mm behind the balance point, with ski-camber profiles (blue lines), apparent pressure distributions (red lines) and elastically deformed counter surfaces (black lines). The vertical red arrow indicates the equivalent loading position and the horizontal black arrow the gliding direction. The elastic moduli used in the simulations are 900 MPa, for the ski base, and 100 MPa, for the (snow) counter surface. Under 30 kg load the ski has a rear/front apparent contact lengths of 146 mm/162 mm with corresponding average apparent pressures of 30.6 kPa/13.8 kPa. Under 60 kg load the ski has a rear/front apparent contact lengths of 288 mm/132 mm with corresponding average apparent pressures of 33.2 kPa/28.9 kPa

Figure 6 illustrates how a change in the load position, i.e., x_m, at full body load $m = 60\,\text{kg}$ and with $E_{counter} = 100\,\text{MPa}$, influences the frictional interface of a classic ski. The load position $x_m = -2.1\,\text{dm}$ is used to represent a skier supporting its weight on the heel of the foot, and as Fig. 6 (left) shows, most of the load will then be distributed over the rear frictional interface. At this load position (210 mm

Preprints (www.preprints.org) | NOT PEER-REVIEWED | Posted: 31 August 2022 doi:10.20944/preprints202208.0512.v1

behind the balance point), the rear/front apparent contact lengths are 200 mm/50 mm, with corresponding average apparent pressures of 56.4 kPa/40.9 kPa, thus defining a 84%/16% load partitioning. Fig. 6 (right) illustrates the case where the load is placed at $x_m = -0.7$ dm, representing the situation where the skier transfers the load forward to collapse the ski and enable using the grip of the kick-wax zone. In this case, the ski camber collapses so that a part of the load is carried inside the kick-wax zone resulting in three load-carrying zones; rear/middle/front. The apparent contact lengths of the rear/middle/front zones are 146 mm/80.9 mm/105 mm with corresponding average apparent pressures of 41.1 kPa/46.6 kPa/34.3 kPa, defining a 45%/28%/27% load partitioning.

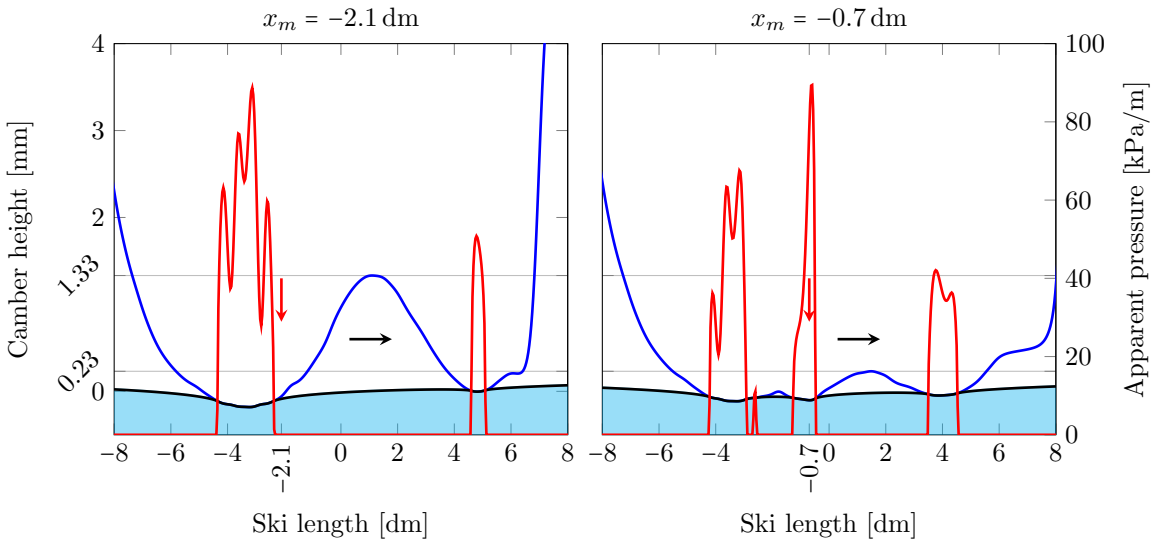

Figure 6: The classic ski under 60 kg of load positioned at 210 mm (left) and 70 mm (right) behind the balance point, with ski-camber profiles (blue lines), apparent pressure distributions (red lines) and elastically deformed counter surfaces (black lines). The vertical red arrow indicates the equivalent loading position and the horizontal black arrow the gliding direction. The elastic moduli used in the simulations are 900 MPa, for the ski base, and 100 MPa, for the snow counter surface. With the load positioned at $x_m = -210$ mm the rear/front apparent contact lengths of 200 mm/51 mm with corresponding average apparent pressures of 56.4 kPa/40.9 kPa. With the load positioned at $x_m = -70$ mm, the there are three contact zones; rear/middle/front, with apparent contact lengths and corresponding average apparent pressures 146 mm/80.9 mm/105 mm and 41.1 kPa/46.6 kPa/34.3 kPa, respectively.

Figure 7 illustrates results simulating the effect that different snow conditions might have on the apparent contact length and pressure. To this end, contact mechanics calculations are conducted with two different elastic moduli of the counter surface, i.e., $E_{counter} = 50$ MPa and 200 MPa. Recall that the ski-camber profiles are identical for a given load case, but, in order to fulfil moment balance (3), they have to be rotated slightly differently when the elastic modulus is changed. For the "softer snow condition", simulated with $E_{counter} = 50$ MPa, the apparent pressure is lower while the apparent contact area and penetration depths are larger than for the "stiffer snow condition", simulated with $E_{counter} = 200$ MPa. It is noted that the rear/front apparent contact area reduces from 141 mm/74 mm to 98 mm/37 mm, expressing a 31%/50% decrease. Comparing with the simulations representing a counter surface made of stone, i.e., $E_{counter} = 70$ GPa, depicted in Fig. 4, the rear/front apparent contact area reduces additionally with 71%/60% to 28.1 mm/14.9 mm.

Preprints (www.preprints.org) | NOT PEER-REVIEWED | Posted: 31 August 2022 doi:10.20944/preprints202208.0512.v1

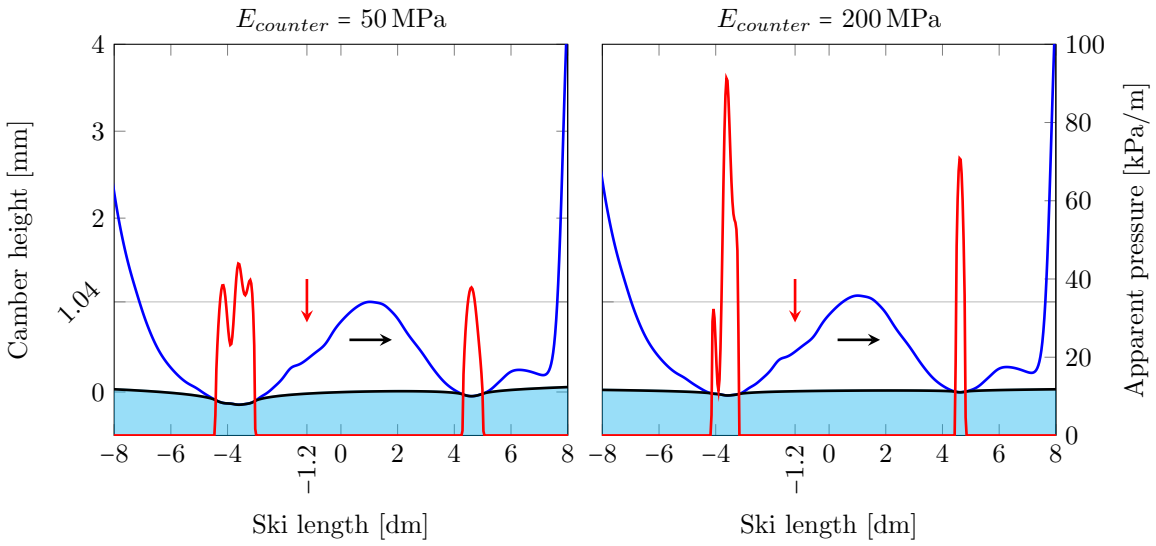

Figure 7: The classic ski under a load of 30 kg positioned 120 mm behind the balance point, supported by snow of two different elastic modules, $E_{counter}$ = 50 MPa (left) and $E_{counter}$ = 200 MPa (right), with corresponding ski-camber profiles (blue lines), pressure distributions (red lines) and elastic deformation (black line). The vertical red arrow indicates the equivalent loading position and the horizontal black arrow the gliding direction. The elastic modulus of the ski base used in the simulations is 900 MPa. Contact with snow having elastic modulus of 50 MPa results in a rear/front apparent contact lengths of 141 mm/74 mm with corresponding average apparent pressures of 33.3 kPa/27.2 kPa. Contact with snow having elastic modulus of 200 MPa results in a rear/front apparent contact lengths of 98 mm/37 mm with corresponding average pressures of 48.2 kPa/52.7 kPa.

As apparent contact pressure and area are closely connected to friction, it is important to know how they vary with the elastic modulus of the snow counter surface and the load exerted by the skier on the ski. Figure 8 depicts the apparent contact area (in [cm^2]) for the rear- (left) and front- (right) frictional interfaces, of the skate ski (with results previously presented in Fig. 4 and 5), as a function of the applied load on the ski (m). Each of the contours, which are spaced by 20 MPa, shows the result for different elastic modulus of the counter surface ($E_{counter}$). The thick solid black line corresponds to the apparent contact area estimate obtained with the Breitschädel contact criterion [26], based on the assumption that contact occurs wherever the ski-camber height is less than 50 µm. The solid green, blue and red lines correspond to the counter surfaces with elastic modulus of 20, 260 and 400 MPa.

The rear frictional interface has, in general, an increasing apparent contact area with increasing load, see Fig. 8 (left). For values of $E_{counter}$ higher than 260 MPa, there is, however, a local maximum at about 35 to 40 kg and thereafter the apparent contact area attains a local minimum at about 40 to 45 kg before it begins increasing again. The estimate of the apparent contact area of the rear frictional interface, obtained using Breitschädel contact criterion, follows a similar trend for elastic moduli within the range 50 - 150 MPa and for loads higher than 20 kg, but exhibits a very different behaviour for lower loads than that.

According to Fig. 8(right), the apparent contact area of the front frictional interface increases with increasing load up to about 30 kg for all loads and elastic moduli within the conditions simulated. For $E_{counter}$ > 40 MPa a local maxima appears, which converges to about 50 cm^2 at 30 kg as $E_{counter} \longrightarrow$ 400 MPa. Thereafter, it decreases somewhat to plateau out at a more-or-less constant level. The explanation

Preprints (www.preprints.org) | NOT PEER-REVIEWED | Posted: 31 August 2022 doi:10.20944/preprints202208.0512.v1

has to do with what can be seen in Fig. 5, where the front frictional interface under a load of 30 kg consists of a single patch while it at 60 kg has separated into two. For $E_{counter} > 260$ MPa the splitting from one to two patches occurs at a load of approximately 35 kg. For the front frictional interface, the Breitschädel contact criterion quite closely follows the present prediction for $E_{counter} = 20$MPa, at least except for at the high end of the load range. Thus, according to the present approach, Breitschädel's contact criterion, may be to predict the (total) apparent contact area for "soft snow" conditions, rather accurately. A notable difference between the rear- and front frictional interfaces, is that the apparent contact area at the rear frictional interface increases with the load after passing the local minimum, whereas the apparent contact area at the front frictional interface remains almost constant within the same range of loads.

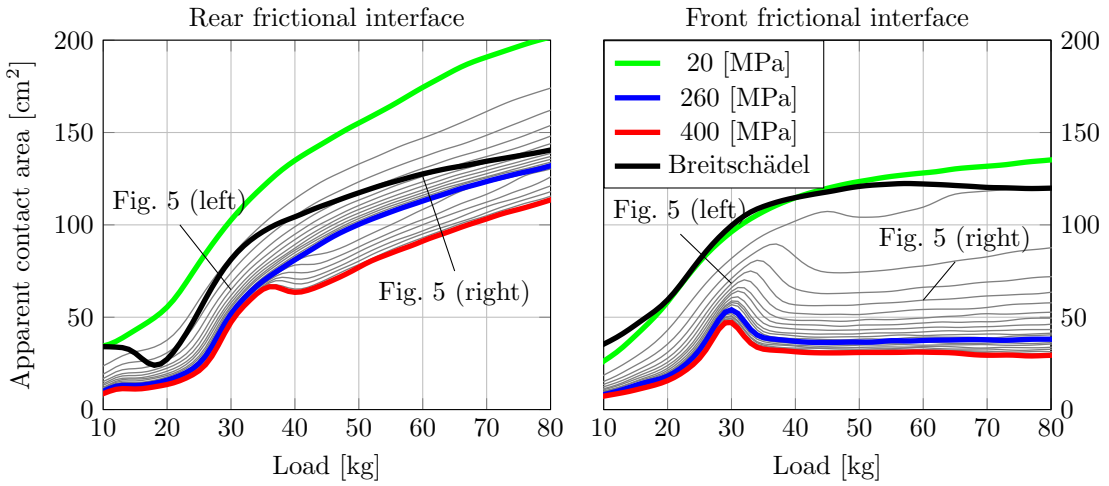

Figure 8: The apparent contact area of the rear- (left) and front- (right) friction interface of the skate ski from Fig. 5 and 4. The apparent contact area of the rear- (left) and front- (right) friction interface, considered as a function of the load magnitude m. The load is placed 120 mm behind the balance point and the contours corresponds to the elastic modulus of the counter surface $E_{counter}$, which is varied from 20 to 400 MPa with increments of 20 MPa. The solid black line corresponds to the apparent contact area determined by utilising the Breitschädel contact criterion [26].

Figure 9 depicts the average apparent contact pressure corresponding to the apparent contact area depicted in Fig. 8. For the same load where the local maximum of the apparent contact area of the rear frictional interface could be observed in Fig. 8, a global minimum in the mean apparent contact pressure can be found. For the rear frictional interface, see Fig. 9 (right), the apparent contact pressure remains almost constant for loads higher than 30 kg, and this is since that the apparent contact area exhibits an almost linear increase within this range of loads. Due to the steady increase in contact area, the pressure at loads higher than 30 kg does not exceed 55 MPa, even for the "stiffest snow" condition simulated using $E_{counter} = 400$ MPa. The apparent contact pressure of the front frictional interface, see Fig. 9 (left), decreases with increasing load until reaching a global minimum at approximately 30 kg. This minimum, corresponding to the local maximum in the apparent contact area, is clearly pronounced for $E_{counter} > 200$ MPa but also existent for smaller values. After this the pressure increases more-or-less linearly with increasing load, as suggested by the almost constant area depicted in Fig. 8.

Preprints (www.preprints.org) | NOT PEER-REVIEWED | Posted: 31 August 2022 doi:10.20944/preprints202208.0512.v1

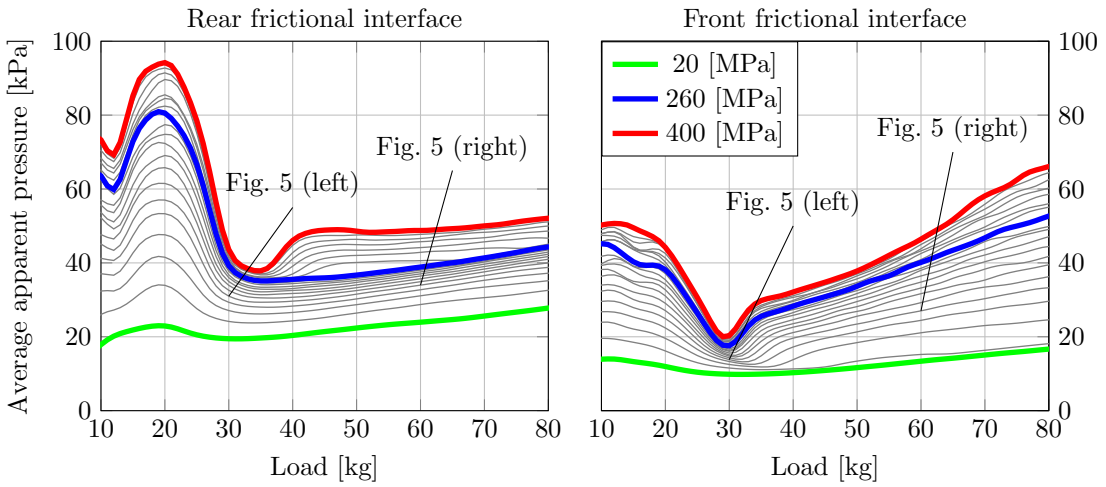

Figure 9: The average apparent pressure of the rear- (left) and front- (right) friction interface, considered as a function of the load magnitude m, and corresponding to the apparent contact areas in Fig. 8. The load is placed 120 mm behind the balance point and the contours corresponds to the elastic modulus of the counter surface $E_{counter}$, which is varied from 20 to 400 MPa with increments of 20 MPa.

The skate ski used herein has, in fact, belonged to and been used by an elite female skier who has a body weight of approximately 60 kg. It is, therefore, quite interesting to see that there is some sort of "sweet spot" around 30 kg, which corresponds to the situations where the athlete distributes the weight evenly on both skis. What this actually means is that at a load corresponding to half of the skiers body weight, the apparent contact area and average apparent contact pressure remains almost the same for a large range of snow conditions, represented here by $E_{counter}$ = 260 MPa - 400 MPa, whereas at full body weight, i.e., 60 kg, there will be a large difference in the apparent contact area and average apparent contact pressure.

5 Conclusions

Concluding the results herein, it can be said that a measurement sequence with varying load magnitude and position can be used as training data for an Artificial neural network (ANN). A feasible ANN trained on such a data set, consisting of measured ski-camber profiles collected with a SkiSelector [30], for various load conditions was also developed. A well-established deterministic BEM based contact mechanics model was adopted and further modified to simulate the contact between a classic- and a skate ski with a counter surface modelled as an elastic half space. To test the model's feasibility, an initial test, in which the contact between the ski and the stone in the SkiSelector, was carried out. The model was then used to predict the contact mechanical response for both the classic- and the skate ski, for a wide range of load conditions and with different elastic moduli of the counter surface. The main findings from employing the present BEM based approach to perform simulations on the two selected skis are listed below.

- The apparent contact area and the apparent contact pressure for a given loading condition can be calculated using the present model.
- The predictions made for the contact mechanics response of the skate ski, shows how the apparent contact area of the front frictional interface splits up from one into two patches as the load increases.
- The predictions made of the contact mechanics response for the classic ski, shows how the ski camber

collapses when the load is transferred forward and that a part of the load is then carried inside the kick-wax zone resulting in three load-carrying zones.

- The apparent contact area of the front frictional interface has a local maximum at a load of approximately half the skiers body weight, and the apparent contact area remains almost constant for loads higher than that.
- The average apparent contact pressure at both the rear- and front frictional interfaces exhibit minima at a load of approximately half the skiers body weight.
- The steady increase in apparent contact area with increasing load, leads to that the average apparent contact pressure at loads higher than half of the body weight remains limited (below 55 MPa), even for the "stiffest snow" condition simulated (using $E_{counter}$ = 400 MPa).

Acknowledgement

The authors would like to acknowledge the support from SOK (The Swedish Olympic Committee) and from VR (The Swedish Reseach Council): DNR 2019-04293.

Author Contribution

Conceptualization, K.K., R.L. and A.A.; methodology, K.K.; software, K.K.; validation, K.K.; formal analysis, K.K.; investigation, K.K.; resources, K.K., J.S. and G.H..; data curation, K.K.; writing—original draft preparation, K.K., J.S., G.H., R.L., H.H. and A.A.; writing—review and editing, K.K., J.S., G.H., R.L., H.H. and A.A.; visualization, K.K., J.S. and G.H.; supervision, R.L., H.H. and A.A.; project administration, A.A.; funding acquisition, R.L., H.H. and A.A. All authors have read and agreed to the published version of the manuscript.

References

1. Bowden, F. The mechanism of sliding on ice and snow. *Proceedings of the Royal Society of London. Series A. Mathematical and Physical Sciences* **172,** 280–298. ISSN: 0080-4630, 2053-9169. https://royalsocietypublishing.org/doi/10.1098/rspa.1939.0104 (2021) (Aug. 1939).
2. Eriksson, R. Friction of runners on snow and ice. Swedish (1949).
3. Bowden, F. P. Some Recent Experiments in Friction: Friction on Snow and Ice and the Development of some Fast-Running Skis. *Nature* **176,** 946–947. ISSN: 0028-0836, 1476-4687. http://www.nature.com/articles/176946a0 (2021) (Nov. 1955).
4. Glenne, B. Sliding Friction and Boundary Lubrication of Snow. *Journal of Tribology* **109,** 614–617. ISSN: 0742-4787, 1528-8897. https://asmedigitalcollection.asme.org/tribology/article/109/4/614/433630/Sliding-Friction-and-Boundary-Lubrication-of-Snow (2021) (Oct. 1987).
5. Lehtovaara, A. *Kinetic friction between ski and snow* (Jan. 1989).
6. Bejan, A. The Fundamentals of Sliding Contact Melting and Friction. *Journal of Heat Transfer* **111,** 13–20. ISSN: 0022-1481. eprint: https://asmedigitalcollection.asme.org/heattransfer/article-pdf/111/1/13/5910218/13_1.pdf. https://doi.org/10.1115/1.3250635 (Feb. 1989).
7. Bejan, A. in *Advances in Heat Transfer* 1–38 (Elsevier, 1994). ISBN: 978-0-12-020024-5. https://linkinghub.elsevier.com/retrieve/pii/S0065271708702314 (2021).
8. Makkonen, L. Application of a new friction theory to ice and snow. *Annals of Glaciology* **19,** 155–157. ISSN: 0260-3055, 1727-5644. https://www.cambridge.org/core/product/identifier/S0260305500011149/type/journal_article (2021) (1994).

9. Matveev, K. I. An analytical model for flat-ski friction in steady horizontal gliding. *Sports Engineering* **20,** 293–298. ISSN: 1369-7072, 1460-2687. http://link.springer.com/10.1007/s12283-017-0229-y (2021) (Dec. 2017).
10. Lever, J. H., Taylor, S., Hoch, G. R. & Daghlian, C. Evidence that abrasion can govern snow kinetic friction. *Journal of Glaciology* **65,** 68–84. ISSN: 0022-1430, 1727-5652. https://www.cambridge.org/core/product/identifier/S0022143018000977/type/journal_article (2021) (Feb. 2019).
11. Lever, J. H., Asenath-Smith, E., Taylor, S. & Lines, A. P. Assessing the Mechanisms Thought to Govern Ice and Snow Friction and Their Interplay With Substrate Brittle Behavior. *Frontiers in Mechanical Engineering* **7,** 690425. ISSN: 2297-3079. https://www.frontiersin.org/articles/10.3389/fmech.2021.690425/full (2021) (June 2021).
12. Scherge, M., Stoll, M. & Moseler, M. On the Influence of Microtopography on the Sliding Performance of Cross Country Skis. *Frontiers in Mechanical Engineering* **7,** 659995. ISSN: 2297-3079. https://www.frontiersin.org/articles/10.3389/fmech.2021.659995/full (4th May 2021).
13. Almqvist, A. *et al.* A Scientific Perspective on Reducing Ski-Snow Friction to Improve Performance in Olympic Cross-Country Skiing, the Biathlon and Nordic Combined. *Frontiers in Sports and Active Living* **4,** 844883. ISSN: 2624-9367. https://www.frontiersin.org/articles/10.3389/fspor.2022.844883/full (2022) (Mar. 2022).
14. Persson, B. N. J. Elastoplastic Contact between Randomly Rough Surfaces. *Phys. Rev. Lett.* **87,** 116101. https://link.aps.org/doi/10.1103/PhysRevLett.87.116101 (11 Aug. 2001).
15. Yang, C., Tartaglino, U. & Persson, B. N. A multiscale molecular dynamics approach to contact mechanics. *The European Physical Journal E* **19,** 47–58. ISSN: 1292-8941, 1292-895X. https://link.springer.com/10.1140/epje/e2006-00004-9 (2022) (Jan. 2006).
16. Persson, B. Contact mechanics for randomly rough surfaces. *Surface Science Reports* **61,** 201–227. ISSN: 01675729. https://linkinghub.elsevier.com/retrieve/pii/S0167572906000410 (2022) (June 2006).
17. Goryacheva, I. G. *Multiscale Modelling in Contact Mechanics* in *IUTAM Symposium on Scaling in Solid Mechanics* (ed Borodich, F.) (Springer Netherlands, Dordrecht, 2009), 123–134. ISBN: 978-1-4020-9033-2.
18. Yastrebov, V. A., Anciaux, G. & Molinari, J.-F. The role of the roughness spectral breadth in elastic contact of rough surfaces. *Journal of the Mechanics and Physics of Solids* **107,** 469–493. ISSN: 00225096. https://linkinghub.elsevier.com/retrieve/pii/S0022509617303010 (2022) (Oct. 2017).
19. Aramfard, M., Pérez-Ràfols, F. & Nicola, L. A 2D dual-scale method to address contact problems. *Tribology International* **171,** 107509. ISSN: 0301679X. https://linkinghub.elsevier.com/retrieve/pii/S0301679X22000822 (2022) (July 2022).
20. Bäurle, L., Kaempfer, T., Szabó, D. & Spencer, N. Sliding friction of polyethylene on snow and ice: Contact area and modeling. *Cold Regions Science and Technology* **47,** 276–289. ISSN: 0165232X. https://linkinghub.elsevier.com/retrieve/pii/S0165232X06001625 (2021) (Mar. 2007).
21. Mössner, M., Hasler, M. & Nachbauer, W. Calculation of the contact area between snow grains and ski base. *Tribology International* **163,** 107183. ISSN: 0301679X. https://linkinghub.elsevier.com/retrieve/pii/S0301679X21003315 (2021) (Nov. 2021).
22. Bäckström, M., Dahlen, L. & Tinnsten, M. in *The Engineering of Sport 7* 543–549 (Springer Paris, Paris, 2008). ISBN: 978-2-287-09412-5 978-2-287-09413-2. http://link.springer.com/10.1007/978-2-287-09413-2_66 (2021).
23. Schindelwig, K., Hasler, M., Van Putten, J., Rohm, S. & Nachbauer, W. Temperature Below a Gliding Cross Country Ski. *Procedia Engineering* **72,** 380–385. ISSN: 18777058. https://linkinghub.elsevier.com/retrieve/pii/S1877705814005815 (2021) (2014).
24. Kristiansen, P. *Prototyping a measurement device for evaluating the performance of cross-country skis Investigation of pressure-distribution* MA thesis (Oslo, 2019). https://www.duo.uio.no/bitstream/handle/10852/70770/petteakr_masterthesis_final.pdf?sequence=1.
25. Breitschädel, F. Effects of temperature change on cross-country ski characteristics. *Procedia Engineering,* 6 (2010).

26. Breitschädel, F. Variation of Nordic Classic Ski Characteristics from Norwegian national team athletes. *Procedia Engineering* **34,** 391–396. ISSN: 18777058. https://linkinghub.elsevier.com/retrieve/pii/S1877705812016803 (2021) (2012).
27. Kalliorinne, K. TuckThe influence of cross-country skiers' tucking position on ski-camber profile, apparent contact area and the load partitioning. *Part P: Journal of Sports Engineering and Technology,* 7 (2022).
28. Pellegrini, B., Stöggl, T. L. & Holmberg, H.-C. Developments in the biomechanics and equipment of Olympic cross-country skiers. *Frontiers in Physiology* **9,** 976. ISSN: 1664-042X. https://www.frontiersin.org/article/10.3389/fphys.2018.00976/full (2021) (July 2018).
29. Pellegrini, B. *et al.* Methodological Guidelines Designed to Improve the Quality of Research on Cross-Country Skiing. *Journal of Science in Sport and Exercise.* ISSN: 2096-6709, 2662-1371. https://link.springer.com/10.1007/s42978-021-00112-6 (2021) (June 2021).
30. *SkiSelector, SkiSelector Sportdata AB, Piteå, Sweden* http://www.skiselector.com.
31. Kalliorinne, K. *Fischer_Speedmax_3D_Classic_Net_2I* https://www.mathworks.com/matlabcentral/fileexchange/114250-fischer_speedmax_3d_classic_net_2i (2022).
32. Kalliorinne, K. *Fischer_Speedmax_3D_Skate_Plus_Net_2I* https://www.mathworks.com/matlabcentral/fileexchange/114255-fischer_speedmax_3d_skate_plus_net_2i (2022).
33. *Speedmax 3D Classic/Skate, Fischer Sports GmbH, Ried im Innkreis, Austria* https://www.fischersports.com.
34. MATLAB. *9.11.0 (R2021b)* (The MathWorks Inc., Natick, Massachusetts, 2021).
35. Almqvist, A., Sahlin, F., Larsson, R. & Glavatskih, S. On the dry elasto-plastic contact of nominally flat surfaces. *Tribology International* **40,** 574–579. ISSN: 0301679X. https://linkinghub.elsevier.com/retrieve/pii/S0301679X05003142 (2022) (Apr. 2007).
36. Sahlin, F., Larsson, R., Almqvist, A., Lugt, P. M. & Marklund, P. A mixed lubrication model incorporating measured surface topography. Part 1: Theory of flow factors. *Proceedings of the Institution of Mechanical Engineers, Part J: Journal of Engineering Tribology* **224,** 335–351. ISSN: 1350-6501, 2041-305X. http://journals.sagepub.com/doi/10.1243/13506501JET658 (2022) (Apr. 2010).
37. Almqvist, A., Campana, C., Prodanov, N. & Persson, B. N. J. Interfacial Separation between Elastic Solids with Randomly Rough Surfaces: Comparison between Theory and Numerical Techniques. *Journal of the Mechanics and Physics of Solids* **59,** 2355–2369. ISSN: 0022-5096 (2011).
38. Ghaednia, H. *et al.* A Review of Elastic–Plastic Contact Mechanics. *Applied Mechanics Reviews* **69,** 060804. ISSN: 0003-6900, 2379-0407. https://asmedigitalcollection.asme.org/appliedmechanicsreviews/article/doi/10.1115/1.4038187/367076/A-Review-of-ElasticPlastic-Contact-Mechanics (2022) (Nov. 2017).
39. Tiwari, A., Almqvist, A. & Persson, B. N. J. Plastic Deformation of Rough Metallic Surfaces. *Tribology Letters* **68** (Nov. 2020).
40. Pérez-Ràfols, F. & Almqvist, A. On the Stiffness of Surfaces with Non-Gaussian Height Distribution. *Scientific Reports* **11,** 1863. ISSN: 2045-2322 (Dec. 2021).
41. Kalliorinne, K., Larsson, R., Pérez-Ràfols, F., Liwicki, M. & Almqvist, A. Artificial Neural Network Architecture for Prediction of Contact Mechanical Response. *Frontiers in Mechanical Engineering* **6,** 579825. ISSN: 2297-3079. https://www.frontiersin.org/articles/10.3389/fmech.2020.579825/full (2022) (May 2021).
42. Lintzén, N. & Edeskär, T. Uniaxial Strength and Deformation Properties of Machine-Made Snow. *Journal of Cold Regions Engineering* **29,** 04014020. ISSN: 0887-381X, 1943-5495. http://ascelibrary.org/doi/10.1061/%28ASCE%29CR.1943-5495.0000090 (2022) (Dec. 2015).